Computing failure boundaries by continuation of a two-point boundary value problem

Hinke M. Osinga
Department of Mathematics, the University of Auckland, Auckland, New Zealand
email: h.m.osinga@auckland.ac.nz

ABSTRACT: We propose a novel approach to investigating the parameter dependence of system behaviour for models that are subject to an external force. As a particular example we consider the analytical model of a tied rocking block on an elastic foundation, which exhibits dynamics equivalent to that of a planar, post-tensioned frame on a shake table; we are interested in predicting behaviour of models subject to an aperiodic external force (an earthquake), but in this paper we restrict to periodic external forcings only. The failure boundary separates initial conditions, given by the angle and angular velocity of the rocking block, for which trajectories starting from time 0 move past a given maximum angle (in absolute value) from those that remain in the admissible regime for arbitrarily long time integration. There are no methods to compute such a failure boundary directly. Instead, numerical studies have, so far, applied brute-force simulations over a grid of initial conditions.

This paper presents an efficient method, based on the fact that the failure boundary must consist of initial conditions that graze the maximum-angle line. We set up a two-point boundary value problem (2PBVP) that defines trajectory segments starting from a given initial condition and ending at the maximum angle (or its negative) with zero angular velocity. We use continuation to find a one-parameter family of initial conditions that solve this 2PBVP; more precisely, we compute two continuous curves of solutions, one for the positive and one for the negative maximum angle. The failure boundary is a piecewise-smooth curve composed of a finite subset of bounded segments from these two families. We describe properties of the failure boundary in detail and discuss how parameter variation can cause the admissible regime to split into two disjoint pieces.

KEY WORDS: Post-tensioned frame; Failure boundary; Grazing trajectory; Two-point boundary value problem.

1 BACKGROUND

The possibility of an earthquake is a constant threat in many countries. For example, New Zealand has recently been experiencing quite a number of earthquakes that resulted in minor to severe damage to buildings. Most notorious is the 2011 Christchurch earthquake, which followed a series of earthquakes starting in September 2010; buildings constructed using reinforced concrete suffered only minor to moderate damage in this first series of earthquakes, but 135 of the 833 reinforced-concrete buildings were severely damaged in the earthquake on 22 February 2011, including the complete collapse of two such mid-rise buildings [5].

The system studied here models the behaviour of precast concrete frames with post-tensioned tendons connecting elements. This type of frame is an example of a nonlinear elastic moment resisting frame, which have received a lot of attention in the past two decades, because such frames are capable of exhibiting large deformations while still remaining elastic (although nonlinearly). Experimental tests are very promising, with only a minimal amount of damage observed all the way up to design level, and satisfactory performance up to 50% beyond it [11]. More recently, research has shifted from studying quasi-static and slow dynamic behaviour, to the nonlinear dynamic behaviour at a fast time scale for this class of structures [4]. This works builds upon the mathematical models developed by civil engineers at the University of Bristol [1], [2], [8], [9]. More specifically, we use the model from [1] of a tied rocking block on an elastic foundation as the representative example in this paper. This model is given in non-dimensionalised form by the second-order non-autonomous equation

$$\ddot{\varphi} + 2\gamma\dot{\varphi} + \mu(\varphi) = A\sin(\omega t), \tag{1}$$

which is valid only for the admissible regime $|\,\varphi(t)\,| = 10$. The function $\mu(\varphi)$ is defined as

$$\mu(\varphi) = \begin{cases} \mu_{\leq 1}(\varphi) := \varphi, & |\,\varphi\,| \leq 1, \\ \mu_{>1}(\varphi), & |\,\varphi\,| > 1, \end{cases} \tag{2}$$

with

$$\mu_{>1}(\varphi) := \left(\tfrac{3}{\beta} + \tfrac{12}{\beta^2} + \tfrac{8}{\beta^3}\right)\varphi + \left(3 + \tfrac{9}{\beta} + 6\tfrac{1-\sqrt{\psi}}{\beta^2} - 6\tfrac{\sqrt{\psi}}{\beta^3} - 2\tfrac{\psi\sqrt{\psi}}{\beta^3\varphi^2}\right)\operatorname{sgn}(\varphi),$$

and $\psi = (1+\beta)\left(\varphi^2 + \beta\,|\,\varphi\,|\right)$. Note that $\mu(\varphi)$ is continuous and continuously differentiable at $|\,\varphi\,| = 1$. For the purpose of this short paper, we use the parameters $\beta = 85$ and $\gamma = 0.05$ and we fix the frequency of the periodic ground motion to $\omega = 0.575$; see [1] for more details on this model.

The dynamics of system (1) is equivalent to that of a planar, post-tensioned frame on a shake table [1], and the force term on the right-hand side of this equation can be thought of as the

ground motion. System (1) provides information about the post-earthquake structural integrity of the frame for any given forcing amplitude A and frequency ω. In particular, we are interested in the safe region

$$\mathscr{B}_\infty := \{|\,\varphi(t)\,| < 10, \text{ for all } 0 \le t \le T_{\text{end}}\}, \tag{3}$$

where T_{end} is some maximum integration time representing the total duration of the earthquake.

Our goal is to compute the boundary of $\mathscr{B}_\infty$. In [1] this was done with a brute-force simulation that integrates system (1) over a large grid of initial conditions and selects those points that lie in $\mathscr{B}_\infty$. In this paper, we present a direct approach by computing curves of initial conditions with the special property that their corresponding trajectories graze the boundary $|\,\varphi(t)\,| = 10$ for some time $0 \le t \le T_{\text{end}}$. We use the set-up of a two-point boundary value problem (2PBVP) so that the boundary of $\mathscr{B}_\infty$ can be found by continuation. This idea is based on the general approach of computing invariant manifolds via the continuation of a suitably formulated 2PBVP; see [6] for an overview. We have used these ideas successfully for studying transient effects in neurone models [7], [10]. Here, we apply this same framework to study the transient effect of an earthquake lasting over a time interval $[0, T_{\text{end}}]$.

Initially, we fix $A = 0.6$, for which system (1) has three periodic orbits. Two of these periodic orbits are attracting and one is of saddle type. All three periodic orbits lie in $\mathscr{B}_\infty$, that is, $\varphi(t) \in [-10, 10]$ for all points on the periodic orbits. The main purpose of this paper is to show how the failure boundary, that is, the boundary of $\mathscr{B}_\infty$ is formed by a combination of left- and right-grazing trajectories, that is, trajectories that are tangent to the line $\varphi = -10$ or the line $\varphi = 10$, respectively. We also discuss this for amplitudes just beyond the value $A = 0.6$ to show how the nature of the boundary changes.

This paper is organised as follows. In the next section, we discuss how to set up a two-point boundary value problem and use continuation to trace the families of left- and right-grazing trajectories. We then discuss the properties of the failure boundary for $A = 0.6$ in detail in Section 3. We increase the forcing amplitude A in Section 4 to illustrate how the failure boundary, and thus, how $\mathscr{B}_\infty$ changes with A. Finally, we conclude with a discussion in Section 5.

2 COMPUTING THE FAILURE BOUNDARY

We are interested in computing the failure boundary in the $(\varphi, \dot{\varphi})$-plane of initial conditions at time $t = 0$. Points on one side of this boundary lie in $\mathscr{B}_\infty$, while points on the other side of this boundary correspond to trajectories that will leave the regime $\varphi(t) \in [-10, 10]$ for some $0 < t < T_{\text{end}}$. In the computations discussed here, we used $T_{\text{end}} = 9 \times \frac{2\pi}{\omega}$, where $\frac{2\pi}{\omega}$ is the period of the external forcing.

2.1 Set-up of the two-point boundary value problem

We use a direct approach to compute the failure boundary by considering the families of left- and right-grazing orbits as solutions of a two-point boundary value problem (2PBVP). This 2PBVP is solved with continuation in the software package AUTO [3]. Recall that any trajectory of the non-autonomous system (1) is uniquely defined by selecting values φ and $\dot{\varphi}$ associated with a particular time; we consider points in the $(\varphi, \dot{\varphi})$-plane at time $t = 0$. Trajectories that graze the admissible regime $|\,\varphi(t)\,| = 10$ satisfy the additional constraint $\varphi(T) = \pm 10$ and $\dot{\varphi}(T) = 0$ for some time $t = T$, where $0 \le T \le T_{\text{end}}$ is not known. We formulate these constraints in a 2PBVP set-up of three first-order differential equations with three boundary conditions. To this end, we consider orbit segments $\mathbf{u} = \{\mathbf{u}(s) = (\varphi(sT), \dot{\varphi}(sT)) \mid 0 \le s \le 1\}$, where $t = 0$ if $s = 0$ and $t = T$ if $s = 1$; note that $\mathbf{u}$ is simply a grazing trajectory with rescaled time such that the orbit segment is always defined on the interval $[0, 1]$. This set-up allows us to formulate the moment of grazing as a boundary condition on the end point $\mathbf{u}(1)$. By extending system (1) with one additional equation for time, the system is given as

$$\begin{cases} \dot{\mathbf{u}}(s) &= T\,\mathbf{f}(\mathbf{u}(s), t(s)), \\ \dot{t}(s) &= T, \end{cases} \tag{4}$$

where the total integration time T is treated as a parameter. In total, there are three first-order equations, because $\mathbf{u}(s)$ is a two-dimensional variable. The three boundary conditions are defined as follows:

$$t(0) = 0, \tag{5}$$

$$\mathbf{u}(1) = (\pm 10, 0). \tag{6}$$

Here, boundary condition (5) specifies time at the begin point of the orbit segment, and (6) gives the other two boundary conditions, namely, that the end point of the orbit segment should be a grazing point ($\dot{\varphi} = 0$) on the line $\varphi = 10$ or $\varphi = -10$. The 2PBVP (4)–(6) defines two solution families in the $(\varphi, \dot{\varphi})$-plane for $t = 0$ that are each parametrised by T; one family is the case $\mathbf{u}(1) = (10, 0)$ and the other is the case $\mathbf{u}(1) = (-10, 0)$. Since system (1) is continous, the two solution families are single continuous curves in the $(\varphi, \dot{\varphi})$-plane for $t = 0$.

It is important to realise that solutions $\mathbf{u}$ to the 2PBVP (4)–(6) do not necessarily lie on the boundary of $\mathscr{B}_\infty$, because we only consider the grazing trajectories up to the moment of grazing, at $t = T$, instead of resolving the trajectory until $t = T_{\text{end}}$. In particular, the trajectory corresponding to $\mathbf{u}$ may leave the regime $\varphi \in [-10, 10]$ before time T_{end} is reached, which could be either before or after the moment of grazing. It turns out that solutions with $T \le T_{\text{end}}$ are quite useful and help interpret the structure and geometry of the failure boundary; see already Section 3.

2.2 Start solution for the 2PBVP

To start the continuation of solutions to the 2PBVP (4)–(6) in AUTO [3], one needs to have a first solution. For each of the two cases, we actually know one solution explicitly, namely the initial conditions $(\pm 10, 0)$ at the left- and right-grazing points solve (4)–(6) with $T = 0$. Of course, $(\pm 10, 0)$ are mere points, but as soon as $T > 0$, they give rise to proper orbit segments that correspond to left- or right-grazing trajectories. Hence, for each forcing amplitude A under consideration, we perform two continuation runs: one starting from $(-10, 0)$ and one starting

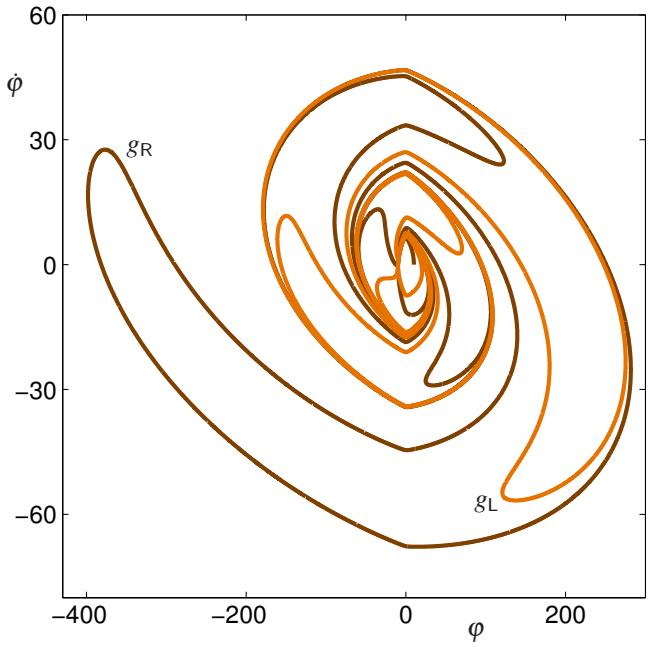

Figure 1. Families of left- and right-grazing trajectories of (1) with $A = 0.6$; the curve of left-grazing trajectories (orange) is labelled g_L and the curve of right-grazing trajectories (brown) is labelled g_R.

from $(10,0)$. Starting from $T = 0$, we continue the 2PBVP (4)–(6) in T until $T = T_{\rm end}$ is reached, at which point we stop the computation.

3 CONTINUATION OF THE 2PBVP WITH $A = 0.6$

As an example, we consider system (1) with $A = 0.6$. We continue the two solution families of the 2PBVP (4)–(6) with AUTO [3], starting from the 'orbit segments' $\{\mathbf{u}(s) = (\pm 10, 0) \mid 0 \le s \le 1\}$, which start and end at $(\pm 10, 0)$, and with $T = 0$; we denote the two families g_L and g_R, indicating whether the grazing is on the left, at $\varphi = -10$, or on the right, at $\varphi = 10$, respectively. Figure 1 shows the corresponding two curves in the $(\varphi, \dot\varphi)$-plane. Even though all points on these two curves correspond to trajectories that graze the lines $\varphi = 10$ (brown curve) or $\varphi = -10$ (orange curve) for some time $0 \le T \le T_{\rm end}$, most of them contain segments that lie well outside the admissible domain $\varphi \in [-10, 10]$. This is the case, because all trajectories converge to either one of the two attracting periodic orbits, which lie in $\mathscr{B}_\infty$. Hence, all initial conditions outside the domain $\varphi \in [-10, 10]$ will eventually enter this domain, and some of these do so while grazing the lines $\varphi = -10$ or $\varphi = 10$. Furthermore, there are also initial conditions that start with $\varphi(0) \in [-10, 10]$, but leave this domain (and then return to it) before the moment of grazing.

The curves g_L and g_R extend forever further in the $(\varphi, \dot\varphi)$-plane as $T_{\rm end}$ increases. However, the boundary of $\mathscr{B}_\infty$ must be contained in the subset of those segments from g_L and g_R that correspond to solutions $\mathbf{u}(s)$ with $|\mathbf{u}(s)| \le 10$ for all $s \in [0, 1]$. In fact, for the case $A = 0.6$, these admissible segments on g_L and g_R satisfy $0 \le T < 4 \times \frac{2\pi}{\omega}$. All points on g_L or g_R with $T \ge 4 \times \frac{2\pi}{\omega}$ already correspond to trajectories that leave the admissible domain before grazing. Hence, the chosen $T_{\rm end} = 9 \times \frac{2\pi}{\omega}$ is more than large enough to find the boundary of $\mathscr{B}_\infty$.

Figure 2 shows only the admissible segments on g_L and g_R, namely, the segments that correspond to trajectories entirely contained in the admissible domain $\varphi \in [-10, 10]$; they all lie in the region $(\varphi, \dot\varphi) \in [-10, 10] \times [-8, 7]$, as shown in panel (a). There are two admissible segments, labelled $g_L^{(0)}$ and $g_R^{(0)}$ that start at $(-10, 0)$ and $(10, 0)$, respectively, and go to the other side of the admissible domain; $g_L^{(0)}$ ends on $\varphi = 10$ and $g_R^{(0)}$ ends on $g_L^{(0)}$, just before reaching $\varphi = -10$. Points on these two segments (roughly) correspond to trajectories that move to the left ($\dot\varphi(0) < 0$) or right ($\dot\varphi(0) > 0$) and immediately leave the admissible domain. The other admissible segments all appear in the top-left corner, and an enlargement of that region, namely, $(\varphi, \dot\varphi) \in [-10, -2.8] \times [-1.3, 6.3]$ is shown in Figure 2(b). The additional segments are labelled as follows. The next segment from g_L that satisfies the constraint $\varphi(t) \in [-10, 10]$ for all $0 \le t \le T$, that is, up to the moment of grazing is labelled $g_L^{(1)}$; the superscript indicates that the trajectories corresponding to points on this segment make (almost) a full rotation with respect to the $(\varphi, \dot\varphi)$-plane. Indeed, most points on $g_L^{(1)}$ satisfy $\dot\varphi(0) > 0$, such that the trajectory first moves to the right, then passes $\dot\varphi(t) = 0$ for some $0 < t < T$ and moves to the left until the moment of grazing with $\varphi(T) = -10$ and $\dot\varphi(T) = 0$; there is a short segment on $g_L^{(1)}$ with $\dot\varphi(0) > 0$, which correspond to trajectories that move through $\dot\varphi(t) = 0$ twice before reaching $\varphi(T_{\rm end}) = -10$ with $\dot\varphi(T_{\rm end}) = 0$. The segments $g_L^{(2)}$ and $g_L^{(3)}$ are defined in the same way; these segments both lie entirely in the region with $\dot\varphi(0) > 0$, and trajectories will pass $\dot\varphi(t) = 0$ three and five times, respectively, before reaching $\varphi(T) = -10$ with $\dot\varphi(T) = 0$. Similarly, the segments $g_R^{(1)}$ and $g_R^{(2)}$ lie entirely in the region with $\dot\varphi(0) > 0$, so that trajectories starting at points on these segments make one and two oscillations, respectively, plus another about half a turn until the moment of grazing with $\varphi(T_{\rm end}) = 10$ and $\dot\varphi(T_{\rm end}) = 0$.

The admissible segments from g_L and g_R intersect at a number of points. More precisely, each additional segment $g_L^{(k)}$ on g_L starts at a point on $g_R^{(0)}$, labelled $\varphi_{\rm RL}^{(0,k)}$ and ends at a point on $g_R^{(k-1)}$, labelled $\varphi_{\rm RL}^{(k-1,k)}$; we gave the last point on $g_L^{(1)}$ label $\varphi_{\rm RL}^{(0,-1)}$, because the label $\varphi_{\rm RL}^{(0,1)}$ is already in use for its first point. All these points correspond to trajectories that satisfy $\varphi(T) = -10$ with $\dot\varphi(T) = 0$, as well as $\varphi(t) = 10$ with $\dot\varphi(t) = 0$, for some $0 < t < T$. Hence, each trajectory has a double grazing, namely, a first one at $\varphi = 10$ and a second one at $\varphi = -10$. These six double-grazing trajectories are shown in Figure 2(c), where the horizontal axis marks integer multiples of the forcing period. As we can see in Figure 2(c), each successive pair of double-grazing orbits makes an additional oscillation, which takes slightly more time than the forcing period $\frac{2\pi}{\omega}$. Note that the trajectories $\varphi_{\rm RL}^{(0,k)}(t)$ satisfy $\varphi = 10$ when $\dot\varphi_{\rm RL}^{(0,k)}(t) = 0$ for the first time, that is, within the first oscillation, while the trajectories $\varphi_{\rm RL}^{(k-1,k)}(t)$, for $k = 2, 3$, graze $\varphi = 10$ only within the $(k-1)$st oscillation.

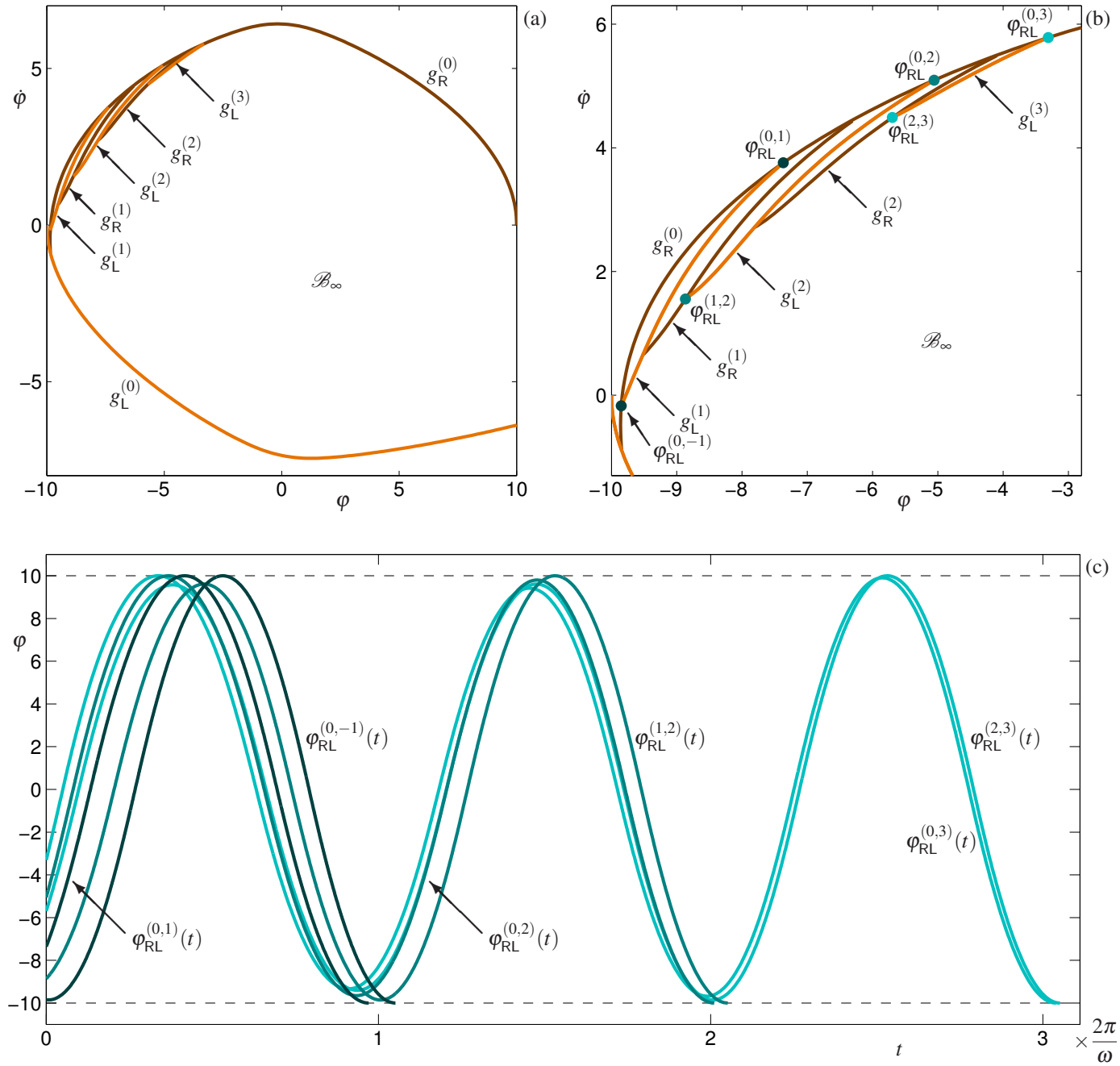

Figure 2. Admissible segments selected from the families g_{L} (orange) and g_{R} (brown), which define the boundary of $\mathscr{B}_\infty$ for $A = 0.6$; the superscripts (k) with $k = 0,1,2,3$ represent the number of oscillations until grazing, as an indication of the moment of grazing at $t = T$. Panel (a) shows all admissible segments and panel (b) is an enlargement that includes the points labelled $\varphi_{\mathsf{RL}}^{(0,k)}$ or $\varphi_{\mathsf{RL}}^{(k-1,k)}$ at which the left-grazing trajectory also grazes the boundary $\varphi = 10$ for some time $t < T$; here, the point on $g_{\mathsf{R}}^{(0)} \cap g_{\mathsf{L}}^{(1)}$ with $\dot\varphi(0) < 0$, is labelled $\varphi_{\mathsf{RL}}^{(0,-1)}$. Time series of these six double-grazing trajectories are shown in panel (c).

The right-grazing segments $g_{\mathsf{R}}^{(k)}$, for $k = 1,2,3$, similarly start at points on $g_{\mathsf{R}}^{(0)}$ and end at points on $g_{\mathsf{L}}^{(k)}$. The first points on $g_{\mathsf{R}}^{(k)}$, $k = 1,2,3$, graze $\varphi = 10$ upon crossing $\dot\varphi = 0$ for the first time and again at $t = T$, while the last points graze $\varphi = -10$ within the kth oscillation and $\varphi = 10$ at $t = T$.

The boundary of $\mathscr{B}_\infty$ itself is piecewise smooth and consists of parts of each of the admissible segments shown in Figure 2. Indeed, a trajectory corresponding to any point above $g_{\mathsf{R}}^{(0)}$ will leave the admissible domain more or less immediately through the line $\varphi = 10$; similarly a trajectory corresponding

to any point below $g_{\mathsf{L}}^{(0)}$ will leave the admissible domain well within the first oscillation through the line $\varphi = -10$. However, points on the other sides of these segments do not necessarily correspond to trajectories that remain inside the admissible domain. For example, points inside the region bounded by $g_{\mathsf{R}}^{(0)}$ and $g_{\mathsf{L}}^{(1)}$ will 'miss' the line $\varphi = 10$, but then leave the admissible domain through the line $\varphi = -10$. Since it takes about half a forcing period to make half an oscillation, the time it takes for these points to leave the admissible domain is about π/ω longer than for nearby points above $g_{\mathsf{R}}^{(0)}$. In other words, the admissible segment $g_{\mathsf{R}}^{(0)}$ marks a line of discontinuity in the time it takes to leave the admissible domain. This discontinuity manifests itself in a complicated way, because the gap is different across each of the segments $g_{\mathsf{L}}^{(k)}$ with $k = 1,2,3$, as well as the segments $g_{\mathsf{R}}^{(1)}$ and $g_{\mathsf{R}}^{(2)}$. For example, points in the region bounded by the three admissible segments $g_{\mathsf{R}}^{(0)}$, $g_{\mathsf{R}}^{(1)}$ and $g_{\mathsf{L}}^{(2)}$ take about $2 \times \frac{2\pi}{\omega}$ to leave the admissible regime, through the line $\varphi = -10$, while points in the region bounded by the three admissible segments $g_{\mathsf{R}}^{(0)}$, $g_{\mathsf{R}}^{(2)}$ and $g_{\mathsf{L}}^{(2)}$ take about $2.5 \times \frac{2\pi}{\omega}$, and leave through the line $\varphi = 10$.

It is this alternating behaviour of trajectories leaving through the lines $\varphi = -10$ and $\varphi = 10$ that characterises the piecewise-smooth nature of the boundary of $\mathscr{B}_\infty$; in particular, this is not caused by the fact that system (1), or more precisely, the function $\mu(\varphi)$ given by equation (2) is piecewise smooth. The discontinuities in the second derivative of $\mu(\varphi)$ at $|\varphi| = 1$ cause the slight kinks on the segments $g_{\mathsf{L}}^{(0)}$ and $g_{\mathsf{R}}^{(0)}$ observed in Figure 2(a); these slight kinks occur repetitively along the curves g_{L} and g_{R}, as shown in Figure 1. However, the admissible segments of g_{L} and g_{R} that lie entirely in the regions $|\varphi| > 1$ are all smooth curves (with boundary).

4 INCREASING THE FORCING AMPLITUDE

If we vary the forcing amplitude A, we find a similar set of admissible segments on the curves g_{L} and g_{R} of left- and right-grazing trajectories that collectively define the boundary of $\mathscr{B}_\infty$. Figure 3 shows the admissble segments on g_{L} and g_{R} for $A = 0.61$. This small increase in forcing amplitude creates more admissible segments, namely, there are now six admissible segments on g_{L} and also six on g_{R}. Even though the total area of $\mathscr{B}_\infty$ is somewhat reduced, overall, the situation is much the same as in Figure 2(a): the segment $g_{\mathsf{L}}^{(0)}$ starts on the line $\varphi = -10$ and ends on $\varphi = 10$; the segment $g_{\mathsf{R}}^{(0)}$ starts on the line $\varphi = 10$ and ends on $g_{\mathsf{L}}^{(0)}$; each admissible segment $g_{\mathsf{L}}^{(k)}$ with $k = 1,\ldots,5$ starts on $g_{\mathsf{R}}^{(0)}$ and ends on $g_{\mathsf{R}}^{(k-1)}$; and each admissible segment $g_{\mathsf{R}}^{(k)}$ with $k = 1,\ldots,5$ starts on $g_{\mathsf{R}}^{(0)}$ and ends on $g_{\mathsf{L}}^{(k)}$. As for $A = 0.6$, it is not really necessary to use $T_{\text{end}} = 9 \times \frac{2\pi}{\omega}$, because all left- and right-grazing trajectories with grazing times $T \geq 6 \times \frac{2\pi}{\omega}$ are not admissible. This fact changes when we increase the forcing amplitude to $A = 0.611$.

The situation for $A = 0.611$ is shown in Figure 4. The number of admissible segments has increased again, but now, the segments $g_{\mathsf{L}}^{(7)}$ and $g_{\mathsf{R}}^{(7)}$ do not connect to the segments $g_{\mathsf{R}}^{(6)}$ and $g_{\mathsf{L}}^{(7)}$, respectively. Instead, they end on the line $\varphi = 10$. Similarly, the segment $g_{\mathsf{R}}^{(6)}$ starts on $g_{\mathsf{R}}^{(0)}$ as expected, but ends on the line $\varphi = 10$, and then 'returns' through $\varphi = 10$ before

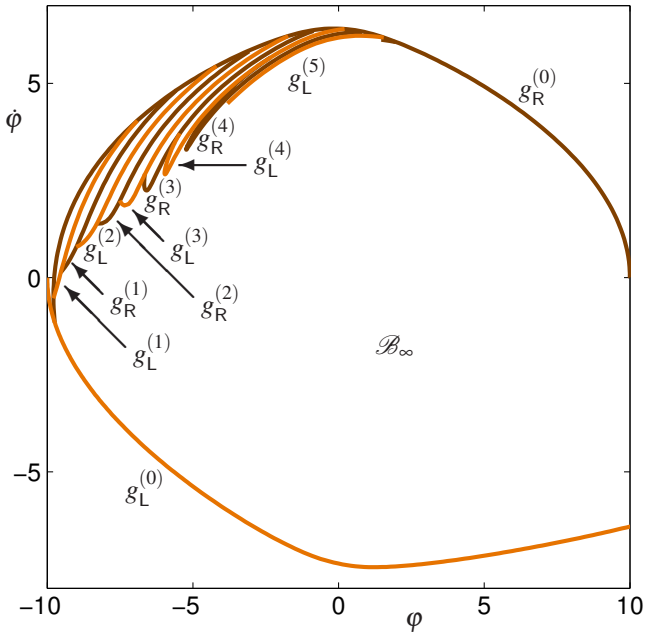

Figure 3. Admissible segments selected from the families g_{L} (orange) and g_{R} (brown) that define the boundary of $\mathscr{B}_\infty$ for $A = 0.61$; the superscripts (k) with $k = 0,1,\ldots,5$ represent the number of oscillations until grazing.

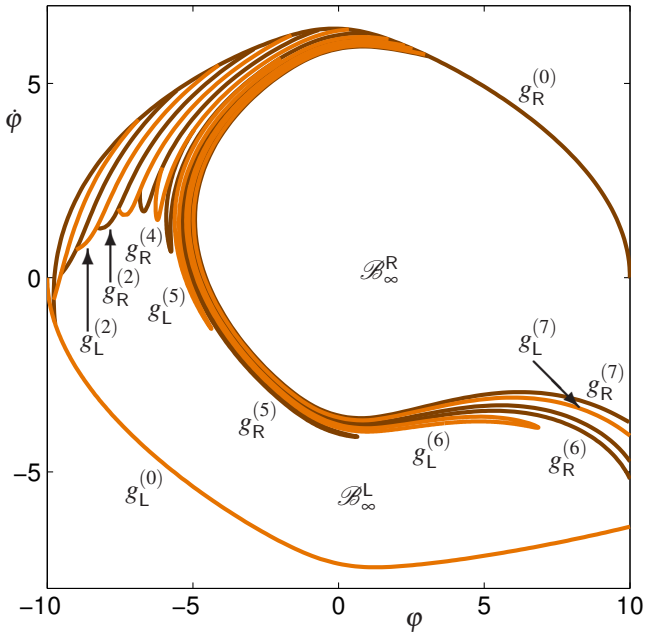

Figure 4. Admissible segments selected from the families g_{L} (orange) and g_{R} (brown) that define the boundary of $\mathscr{B}_\infty^{\mathsf{R}}$ and $\mathscr{B}_\infty^{\mathsf{L}}$ for $A = 0.611$; the superscripts (k) with $k = 0,1,\ldots,7$ represent the number of oscillations until grazing. Note that not all admissible segments are labelled.

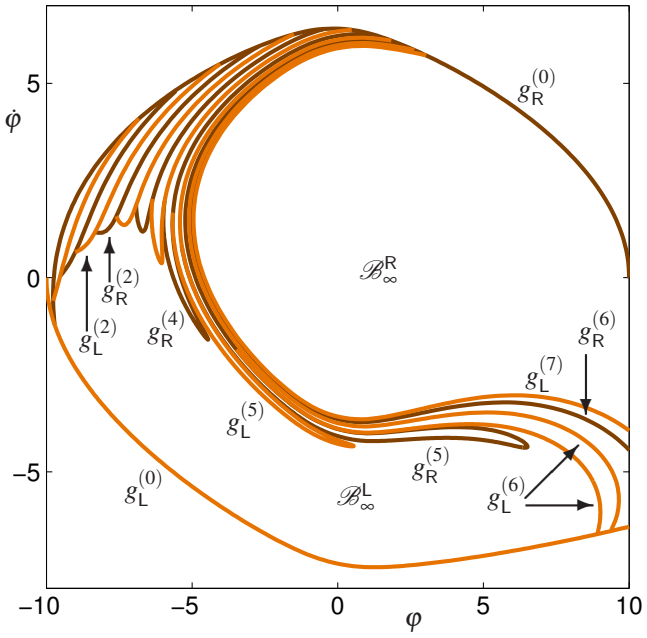

Figure 5. Admissible segments selected from the families g_L (orange) and g_R (brown) that define the boundary of $\mathscr{B}_\infty^R$ and $\mathscr{B}_\infty^L$ for $A = 0.612$; the superscripts (k), with $k = 0, 1, \ldots, 7$ represent the number of oscillations until grazing. Note that not all admissible segments are labelled.

ending on $g_L^{(6)}$; only the latter segment of $g_R^{(6)}$ is labelled in Figure 4. As soon as an admissible segment that starts on $g_R^{(0)}$ ends on the line $\varphi = 10$, the region $\mathscr{B}_\infty$ is no longer connected. It now consists of two regions, which we label $\mathscr{B}_\infty^R$ and $\mathscr{B}_\infty^L$, depending on whether part of the boundary is contained in $g_L^{(0)}$ or in $g_R^{(0)}$, respectively. The region $\mathscr{B}_\infty^L$ is bounded by the admissible segments $g_L^{(0)}$–$g_L^{(6)}$ and $g_R^{(1)}$–$g_R^{(5)}$, together with the first segment of $g_R^{(6)}$ (not labelled in Figure 4). The region $\mathscr{B}_\infty^R$ is bounded by only two admissible segments, namely, $g_R^{(0)}$ and $g_R^{(7)}$. Note that not all admissible segments on g_L and g_R play a role in defining the failure boundary; in particular, $g_L^{(7)}$ nowhere acts as a separatrix.

Apart from the fact that $\mathscr{B}_\infty$ is disconnected for $A = 0.611$, the nature of the failure boundary related to $\mathscr{B}_\infty^R$ has also changed. More precisely, the boundary of $\mathscr{B}_\infty^L$ does not depend on the finite maximal integration time T_{end}; just as for the failure boundaries shown in Figures 2 and 3, it remains the same even if $T_{\text{end}} \to \infty$. However, the boundary of $\mathscr{B}_\infty^R$ does depend on T_{end}. The segments $g_L^{(7)}$ and $g_R^{(7)}$ are the beginning of an accumulation of (ordered) segments $g_L^{(k)}$ and $g_R^{(k)}$, with $k > 7$, that need integration times $T > T_{\text{end}}$. The limit of this accumulation is not an admissible segment on either g_L or g_R, but a finite curve segment on the basin boundary that separates the two attracting periodic orbits (not shown). Hence, in the limit $T_{\text{end}} \to \infty$, the boundary of $\mathscr{B}_\infty^R$ no longer consists solely of left- or right-grazing orbits.

The failure boundary changes rapidly as A increases. Figure 5 shows the situation for forcing amplitude $A = 0.612$. We find that $g_L^{(6)}$ now consists of two segments, but not because this admissible segment ends on $\varphi = 10$, but because it ends on $g_L^{(0)}$. Only the second segment of $g_L^{(6)}$, which starts on $g_L^{(0)}$ and ends on $g_R^{(5)}$, is part of the boundary of $\mathscr{B}_\infty^L$. Hence, the total number of admissible segments that are part of the boundary of $\mathscr{B}_\infty^L$ has decreased. As before, the boundary of $\mathscr{B}_\infty^L$ is independent of T_{end}. On the other hand, the region $\mathscr{B}_\infty^R$ is now bounded by $g_R^{(0)}$ and $g_L^{(7)}$, but this depends on the value chosen for the total integration time T_{end}. Here, the admissible segment $g_R^{(6)}$ plays no role in defining the failure boundary.

5 CONCLUSIONS

We presented a numerical method for the direct computation of the failure boundary. Our approach is to use a two-point boundary value problem set-up and continue curves of left- and right-grazing trajectories in the $(\varphi, \dot{\varphi})$-plane for time $t = 0$. These two families, denoted g_L and g_R, contain segments corresponding to trajectories that lie entirely inside the admissible domain $\varphi \in [-10, 10]$ and the failure boundary is obtained by selecting only those admissible segments. As an example, we used the model of a rocking block on an elastic foundation subject to a periodic force with fixed frequency. We focussed on a small interval of forcing amplitudes near $A = 0.6$. The failure boundary is piecewise smooth, but this is not due to the piecewise-smooth nature of equation (2). It is organised by the fact that the grazing occurs either at the left ($\varphi = -10$) or right ($\varphi = 10$) side of the admissible domain. For small enough forcing amplitudes, the failure boundary is a piecewise-smooth curve that consists of a finite number of segments alternatingly from g_L and g_R and encloses a single region denoted $\mathscr{B}_\infty$. The points at which two admissible segments intersect correspond to double-grazing trajectories. These points also mark a discontinuity along the failure boundary with respect to the total integration time needed to reach the moment of grazing; the discontinuity is roughly given by half the forcing period, because this is about the time needed to complete half of an oscillation. The failure boundary does not depend on the value used for the total integration time T_{end} (provided it is large enough). If the forcing amplitude A increases, the nature of the failure boundary changes. It splits into two piecewise-smooth curves that enclose two regions denoted $\mathscr{B}_\infty^L$ and $\mathscr{B}_\infty^{sfR}$. The boundary of $\mathscr{B}_\infty^L$ is independent of T_{end} and similar in nature to the failure boundaries for smaller A. However, the boundary of $\mathscr{B}_\infty^{sfR}$ now depends on T_{end}. The fact that the failure boundary may enclose two disjoint regions is related to the fact that there are two attracting periodic orbits for our choice of forcing amplitudes. The presence of more than one attractor, of a saddle periodic orbit and its role in changing the nature of the boundary of $\mathscr{B}_\infty^{sfR}$ needs further investigation and will be reported elsewhere.

Our direct computational approach complements brute-force methods that use simulation on a grid of initial conditions. For example, brute-force simulation was used to produce Figure 18

in [1]. In particular, when one compares [1, Figure 18(a)] with Figure 2, which are both for $A = 0.6$, our computed piecewise-wise smooth curve of left- and right-grazing orbit segments precisely delimits the failure boundary obtained from the brute-force simulation. Furthermore, a colour-coding is used in [1, Figure 18(a)] to indicate the integer multiples of the forcing period needed before a trajectory through a given initial condition leaves the admissible regime. Our computations provide information about when the colour changes in [1, Figure 18(a)]. Indeed, the subsets of admissible segments from the families of left- and righ-grazing orbits can also be viewed as discontinuity boundaries in the time it takes to leave the admissible regime $\varphi \in [-10, 10]$. We found that the discontinuity jumps are of the same order as half a period of the forcing, which may explain why the colour seems to change precisely upon crossing admissible segments from the family of right-grazing orbits. These observations need further investigation and will also be reported elsewhere.

ACKNOWLEDGEMENTS

Nick Alexander, Bernd Krauskopf and Sebastian Wieczorek are gratefully acknowledged for fruitful discussions and the generous donation of their time. The observations reported in Section 5 were confirmed by Anna Spyker as part of her summer project at The University of Auckland. This research is supported by a Faculty of Science Research Development Fund from The University of Auckland.

REFERENCES

[1] Alexander N. A., Oddbjornsson O., Taylor C. A., Osinga H. M., Kelly D. E. (2011) Exploring the dynamics of a class of post-tensioned, moment resisting frames. *Journal of Sound and Vibration* **330**(15): 3710–3728.

[2] Dietz M., Oddbjornsson O., Taylor C. A., Ojaghi M., Williams M. S., Blakeborough A. (2010). Shaking table testing of a post-tensioned tendon frame retrofitted with metallic shear panel dissipator. In 9th US/10th Canadian Conference on Earthquake Engineering, Toronto, paper 1185.

[3] Doedel E. J. (2007) AUTO-07P: Continuation and bifurcation software for ordinary differential equations. With major contributions from Champneys A. R., Fairgrieve T. F., Kuznetsov Yu. A., Oldeman B. E., Paffenroth R. C., Sandstede B., Wang X. J., Zhang C.; available at `http://cmvl.cs.concordia.ca/`

[4] Fardis, M. N., Rakicevic, Z. T. (2012) Role of Seismic Testing Facilities in Performance-Based Earthquake Engineering: SERIES Workshop. Springer-Verlag, Dordrecht, Heidelberg, London, New York.

[5] Kam, W. Y., Pampanin, S., Elwood, K. (2011) Seismic performance of reinforced concrete buildings in the 22 February Christchurch (Lyttelton) earthquake. *Bulletin of the New Zealand Society for Earthquake Engineering* **44**(4): 239–278.

[6] Krauskopf, B., Osinga, H. M. (2007) Computing invariant manifolds via the continuation of orbit segments. In Krauskopf, B., Osinga, H. M., Galán-Vioque, J. (Eds.), Numerical Continuation Methods for Dynamical Systems: Path following and boundary value problems, Springer-Verlag, Berlin, pp. 117–154.

[7] Nowacki, J., Osinga, H. M., Tsaneva-Atanasova, K. T. (2013) Continuation-based numerical detection of after-depolarization and spike-adding thresholds. *Neural Computation* **25**(4): 877–900.

[8] Oddbjornsson O., Alexander N. A., Taylor C. A., Sigbjörnsson, R. (2008) Shaking table testing of nonlinear elastic moment resisting frames. In 14th World Conference of Earthquake Engineering, Beijing, paper 11-0110).

[9] Oddbjornsson O., Alexander N. A., Taylor C. A., Sigbjörnsson, R. (2012) Numerical and experimental exploration of the fundamental nonlinear dynamics of self-centring damage resistant structures under seismic excitation. In 15th World Conference of Earthquake Engineering, Lisbon, paper 4670.

[10] Osinga, H. M., Tsaneva-Atanasova, K. T. (2013) Geometric analysis of transient bursts. *Chaos* **23**(4): 046107

[11] Priestley M. J. N., Sritharan S., Conley J. R., Pampanin S. (1999) Preliminary results and conclusiongs from the PRESSS five-story precast concrete test building. *PCI Journal* **44**(6): 42–67.